Alternative analytic method for computing mean observation time in space-telescopes with spin-precession attitude motion

Juan Bermejo-Ballesteros[*1], Javier Cubas[1],
Francisco Casas[2] and Enrique Martínez-González[2]

*[1]Instituto Universitario "Ignacio Da Riva" (IDR/UPM), Universidad Politécnica de Madrid,
Plaza Cardenal Cisneros 3, Madrid, E-28040, Spain*
[2]Instituto de Física de Cantabria (CSIC-UC), Avda. de los Castros s/n, Santander, E-39005, Spain

Abstract. Space-telescopes placed in the Sun-Earth second Lagrange point (L2) observe the sky following a scan strategy that is usually based on a spin-precession motion. Knowing which regions of the sky will be more observed by the instrument is important for the science operations and the instrument calibration. Computing sky observation parameters numerically (discretizing time and the sky) can consume large amounts of time and computational resources, especially when high resolution is required. This problem becomes more critical if quantities are evaluated at detector level instead of considering the instrument entire Field of View (FoV). In previous studies, the authors have derived analytic solutions for quantities that characterize the observation of each point in the sky in terms of observation time according to the scan strategy parameters and the instrument FoV. Analytic solutions allow to obtain results faster than using numerical methods as well as capture detailed characteristics which can be overseen due to discretization limitations. The original approach is based on the analytic expression of the instrument trace over the sky. Such equations are implicit and thus requires the use of numeric solvers to compute the quantities. In this work, a new and simpler approach for computing one of such quantities (mean observation time) is presented. The quantity is first computed for pure spin motion and then the effect of the spin axis precession is incorporated under the assumption that the precession motion is slow compared to the spin motion. In this sense, this new approach further simplifies the analytic approach, sparing the use of numeric solvers, which reduces the complexity of the implementation and the computing time.

Keywords: access time; scan strategy; visibility

1. Introduction

The second Lagrange point (L2) of the Sun-Earth system is a predilected destiny for sky observation missions. This location provides ideal conditions for deep space observations: thermally stable environment, distance from near Earth perturbations (atmosphere, radiation, debris, etc), lack of eclipses and continuous observation of the sky. A significant part of the observation missions planned or already launched to this location (Planck, Gaia, WMAP, LiteBIRD, CORE, or EPIC) cover the whole sky along the year following a scan strategy that determines their attitude motion (Wallis *et al.* 2017, Delabrouille *et al.* 2018, Hazumi *et al.* 2020).

∗Corresponding author, Ph.D. Student, E-mail: juan.bermejo@upm.es

Such motion is usually a combined spin-precession motion, where the satellite spins over one of its axes which rotates around a defined precession axis as shown in Fig. 1.

Commonly, the precession axis is parallel to Sun-Earth line and its positive direction is considered towards deep space (anti-Sun direction). The selection of the scan strategy parameters (α, the separation between spin and precession axes, β, separation of the instrument axis from the spin axis, T_{spin}, spin motion period, and T_{prec}, precession motion period) depends mainly on the scientific objectives and is also subjected to several constraints. For example, the sum of α and β angles must be larger than 90º to cover the whole sky (after half-year) but not so high that the Sun enters the FoV. Other constraints are related to the speed of the spin and the precession motions or their ratio, which will affect different mission aspects such as the sky coverage homogeneity, the required sampling frequency, or the attitude subsystem specifications.

The attitude motion causes the instrument to produce a scan pattern over the sky as the one shown in Fig 2. The instrument pointing direction ($\vec{q}$) can be obtained combining the attitude matrix of the satellite (Eq. (1)) and the instrument mounting matrix (Eq. (2)). By choosing an adequate Euler angle sequence (1-3-1), the attitude matrix of the satellite can be expressed as a function of three of the scan strategy parameters (α, T_{spin} and T_{prec})
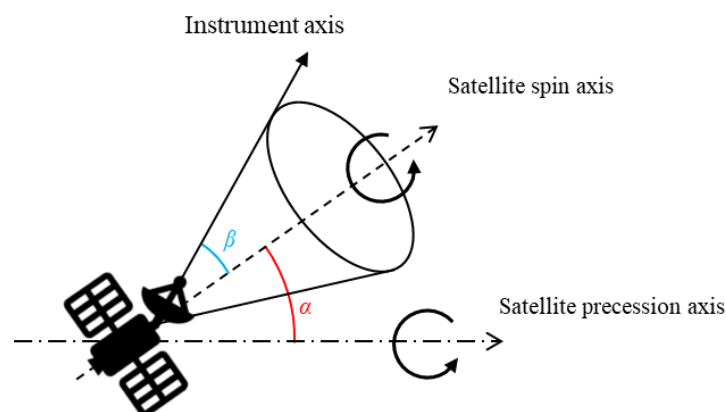

Fig. 1 Scheme of scan strategy based on a spin-precession attitude motion
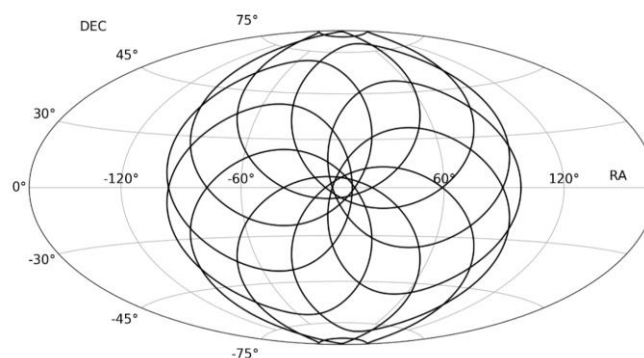

Fig. 2 Hammer projection of the instrument trace over the sky. The center of the projection corresponds to the precession axis

$$C_{sat} = \begin{pmatrix} c_\alpha & c_\xi s_\alpha & s_\xi s_\alpha \\ -c_\psi s_\alpha & c_\psi c_\alpha c_\xi - s_\psi s_\xi & c_\psi c_\alpha s_\xi + s_\psi c_\xi \\ s_\psi s_\alpha & -s_\psi c_\alpha c_\xi - c_\psi s_\xi & -s_\psi c_\alpha s_\xi + c_\psi c_\xi \end{pmatrix} \tag{1}$$

$$\xi = \frac{2\pi}{T_{spin}} t \tag{2}$$

$$\psi = \frac{2\pi}{T_{prec}} t \tag{3}$$

The instrument frame is considered to be rotated an angle β from the satellite frame and its pointing direction to be its X_{inst}-axis

$$C_{inst} = \begin{pmatrix} c_\beta & s_\beta & 0 \\ -s_\beta & c_\beta & 0 \\ 0 & 0 & 1 \end{pmatrix} \tag{4}$$

$$\vec{q}(t) = C_{sat} C_{inst} \begin{Bmatrix} 1 \\ 0 \\ 0 \end{Bmatrix} \tag{5}$$

The geometry of the pattern will depend on the values of the scan strategy parameters. As the instrument follows that path, it will observe those points in the sky that enter its Field of View (FoV). However, it is not intuitive how often this will occur and how long each point will be seen. Normally, this and other parameters to quantitatively assess the quality of a scan strategy are computed directly using numerical methods (Bennet *et al.* 2003, Bock *et al.* 2008, Dupac and Tauber 2004, Kelsall *et al.* 1998), discretizing the sky and the time interval, checking which points are seen each step time and computing the required quantities. The main disadvantage of this approach is that the computational cost grows proportionally to the spatial and temporal discretization., becoming inefficient for studying the impact of the scan strategy parameters on the mission performance. Nevertheless, these methods may be imperative in some cases as with the systematic errors, whose modelling can be too complex to use analytical methods.

In previous studies (Bermejo-Ballesteros *et al.* 2022, 2019, Casas *et al.* 2021) the authors have employed such numerical methods and derived analytic expressions for observation quantities in order to assess the impact of the scan strategy on calibration activities for the telescope. These quantities are defined for each point in the sky (whose position is defined by two angles, θ and φ, as shown in Fig. 3) and characterize the periods of time when such point is inside the instrument FoV (which are called here accesses).

The studied quantities are the sum of all accesses duration (T_{total}), the mean duration of the accesses (T_{mean}), and the maximum duration between all the access (T_{max}). These analytic solutions have been successfully validated against numerical results, require far less computational resources and provide results much faster. The main assumption of the study is that these quantities are symmetric regarding the precession axis. Therefore, if the precession axis coincides with the X_0-axis, these quantities do not depend on θ coordinate, only on φ coordinate. This assumption will be valid as long as the combined period of the spin and precession motion and the period of time considered are high (compared to both motion periods).

In Figs. 4-6, examples of the three quantities are shown. These results have been obtained with the methods presented in Bermejo-Ballesteros *et al.* 2022. The Figs. 4(a), 5(a) and 6(a) show a
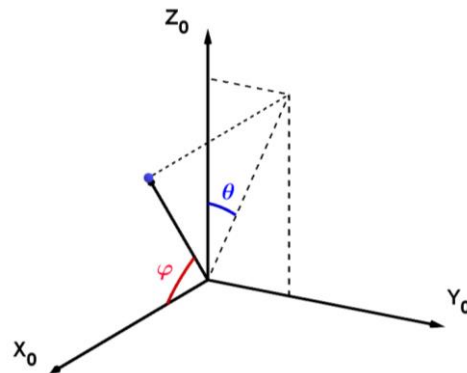
Fig. 3 Coordinates used to describe the position of each point of the sky. The X_0-axis coincides with the precession axis

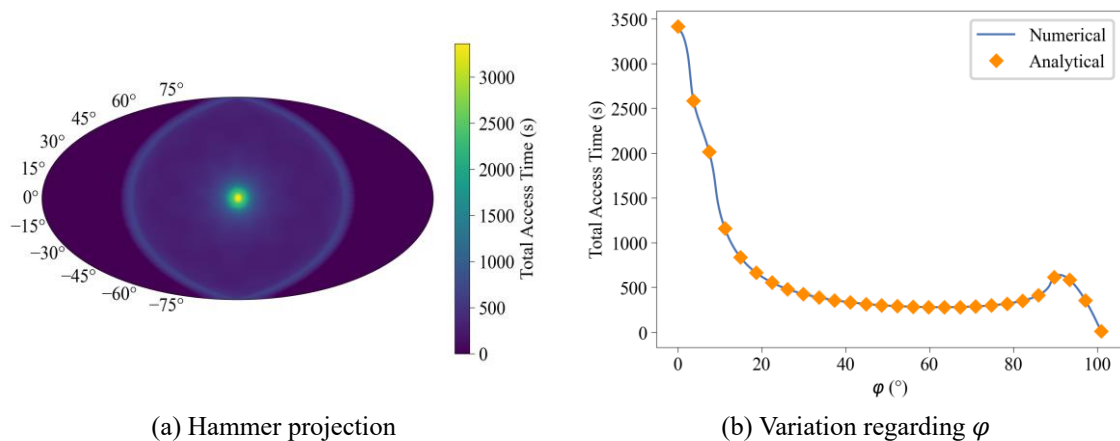(a) Hammer projection   (b) Variation regarding φ

Fig. 4 Total access time

Hammer projection of the numerical results obtained analyzing each point of the discretized sky mesh, where the axial-symmetry around the precession axis can be clearly appreciated. Therefore, these results can be simplified, analyzing the variation of the quantities regarding the φ coordinate, which is shown in the Figs. 4(b), 5(b) and 6(b), where the analytical and numerical results are compared.

The total access time is not affected by the precession as a higher speed will shorten the accesses duration, but it will increase the number of accesses proportionally. Meanwhile, the mean access time and the maximum access time change as the precession speed does, especially for large values of φ coordinate. However, the original approaches followed for the mean access time and the maximum access time to include the precession effect are different. In the former case, the precession motion is considered from the start, analyzing the trace of the instrument while in the latter case, $T_{\max}$ is calculated for a pure spin motion and then the effect of the precession is added using a correction factor which depends on the precession motion and spin motion speeds.

In this work, the correction factor applied for the maximum access time will be applied to the mean access time and the results will be compared against the previous approach and the
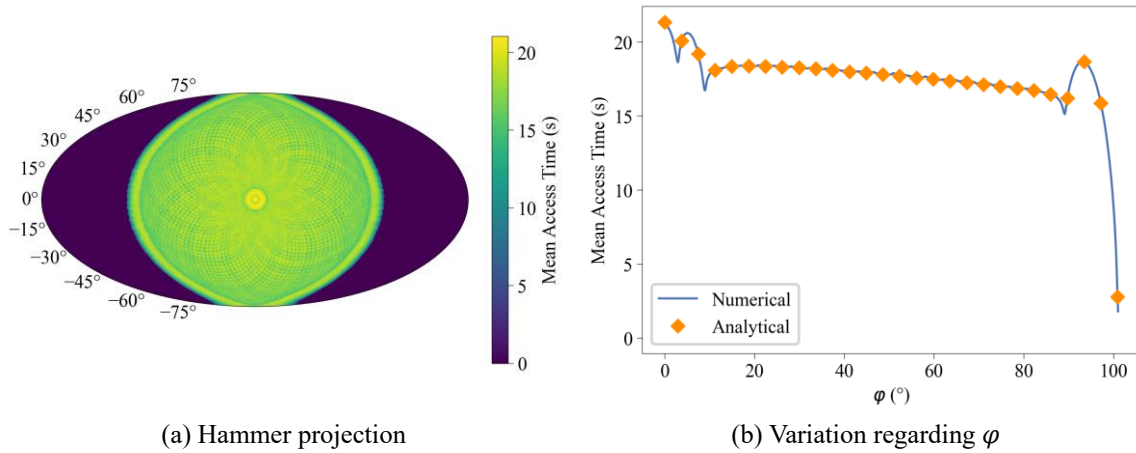
| (a) Hammer projection | (b) Variation regarding φ |

Fig. 5 Mean access time

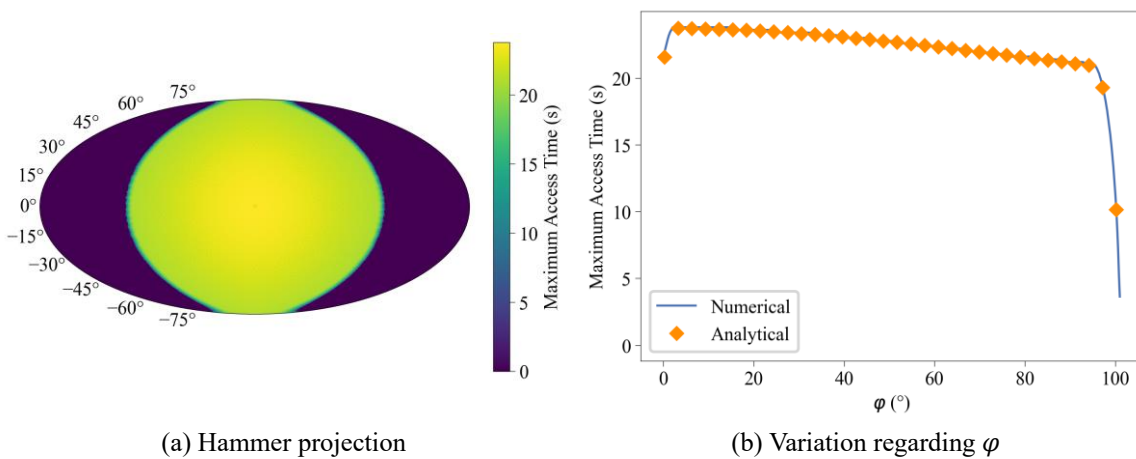| (a) Hammer projection | (b) Variation regarding φ |

Fig. 6 Maximum access time

numerical results. This new approach will simplify the calculation process as it requires less and simpler operations. Furthermore, it will facilitate the software implementation of the approach. The error in all the results is in the same order of magnitude as the numerical time step.

2. Alternative method for T_{MEAN}

In the original approach, the complete motion (spin and precession) is considered to compute T_{mean}. This requires evaluating the derivate of the expression that determines the instrument pointing (Eq. (5)) and find the root of nonlinear functions (Eqs. (15)-(18)). With the new approach, this is avoided, requiring only the evaluation of explicit formulas. This is achieved by making the assumption that the precession motion is slow compared to spin motion, which allows to decouple the effect of both motions. Thus, T_{mean} is computed for the case of pure spin motion and then its value is corrected by a factor that depends on the spin and precession speeds.

2.1 Original approach

The mean access time is computed by dividing the total access time by the number of accesses. The derivation of the analytical expression for the total access time (Eq. (6)) is not included here for succinctness but it can be found in detail in Bermejo-Ballesteros *et al.* 2022.

$$T_{total}(\varphi) = T_{sim} \frac{1}{\pi} \int_0^\pi \frac{1}{\pi} \text{Re}\left(\arccos\left(\frac{\cos(\delta) - \cos(\varphi_v)\cos(\varphi)}{\sin(\varphi_v)\sin(\varphi)}\right) d\phi\right) \tag{6}$$

where δ is the FoV half-angle and φ_v can be obtained from

$$\varphi_v = \arccos(\cos(\alpha)\cos(\beta) - \sin(\alpha)\sin(\beta)\cos(\phi)) \tag{7}$$

As previously said, the total access time is not affected by the precession speed. However, the number of accesses $N(\varphi)$ does. As the motion is periodic, the proportion of points (f_m) in the sky with the same φ coordinate that have been inside the instrument FoV after a spin period is constant. Thus, the total number of accesses during a given period can be obtained by multiplying the number of spin cycles by f_m.

$$T_{mean}(\varphi) = \frac{T_{total}(\varphi)}{N(\varphi)} \tag{8}$$

$$N(\varphi) = f_m \frac{T_{sim}}{T_{spin}} \tag{9}$$

$$f_m = \frac{2\Delta\theta}{2\pi} \tag{10}$$

$$\Delta\theta = \theta_e - \theta_i \tag{11}$$

To compute f_m for a given φ, the θ coordinates of the intersection points of the interior and exterior curves that delimit the area swept by the instrument FoV are determined (Fig. 7). To do so,
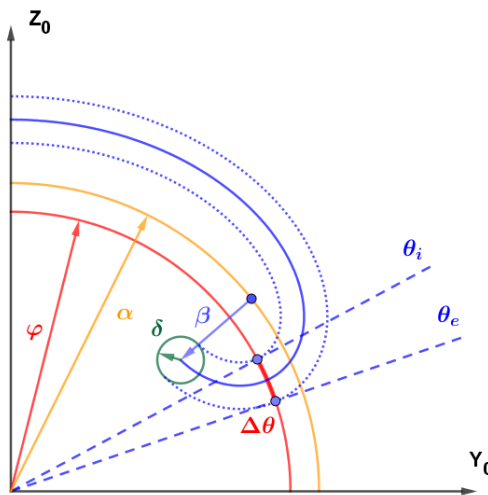

Fig. 7 Geometrical scheme of the instrument trace for a half of T_{spin}. The area swept by the instrument FoV is delimited by two curves parallel to the trace. The angle δ is the half-angle of the FoV

the equations of such curves are obtained from the expression of the instrument pointing over time $\vec{q}(t)$

$$\vec{q}_e(t) = \vec{q}\cos(\delta) + \vec{n}\sin(\delta) = \begin{pmatrix} x_e(t) \\ y_e(t) \\ z_e(t) \end{pmatrix} \tag{12}$$

$$\vec{q}_i(t) = \vec{q}\cos(\delta) - \vec{n}\sin(\delta) = \begin{pmatrix} x_i(t) \\ y_i(t) \\ z_i(t) \end{pmatrix} \tag{13}$$

$$\vec{n} = \frac{\vec{q}'(t)^{\wedge}\vec{q}(t)}{|\vec{q}'(t)|} \tag{14}$$

with $\vec{n}$ being the unitary normal to the instrument trace $\vec{q}(t)$, whose expression has been derived in the previous section.

$$\varphi_e(t) = \text{Re}\big(\arccos(y_e(t))\big) \tag{15}$$

$$\theta_e(t) = \text{Re}\left(\arccos\left(\frac{z_e(t)}{\sin(\varphi_e(t))}\right)\right) \tag{16}$$

$$\varphi_i(t) = \text{Re}\big(\arccos(y_i(t))\big) \tag{17}$$

$$\theta_i(t) = \text{Re}\left(\arccos\left(\frac{z_i(t)}{\sin(\varphi_i(t))}\right)\right) \tag{18}$$

Such expressions are solved to find the instant when both curves reach the coordinate φ. Then, the coordinates θ_e and θ_i are computed for the resulting time and thus the value of $T_{mean}(\varphi)$ can be computed. A summary of the steps is shown in Fig. 8.
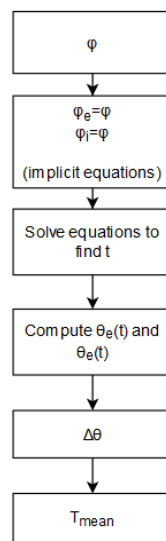

Fig. 8 Scheme of the steps followed to compute T_{mean} using the original approach

2.1 New approach

In this approach, first T_{mean} for negligible precession is calculated. In such case, the trace can be approximated as a circle (due to the spin motion) that slowly rotates around the precession axis (Fig. 10(a)). This allows to simplify the calculation of θ_e and θ_i, for which analytic solutions can be found

$$\theta_e|_\varphi = \text{Re}\left(\arccos\left(\frac{\cos(\beta + \delta) - \cos(\alpha)\cos(\varphi)}{\sin(\alpha)\sin(\varphi)}\right)\right) \tag{19}$$

$$\theta_i|_\varphi = \text{Re}\left(\arccos\left(\frac{\cos(\beta - \delta) - \cos(\alpha)\cos(\varphi)}{\sin(\alpha)\sin(\varphi)}\right)\right) \tag{20}$$

These expressions allow to compute directly the θ coordinate of the interior and exterior curves from the area swept by the instrument for a given φ. An example of the result obtained for T_{mean} when precession is negligible is shown in Fig. 9.

Then, considering that the instrument sweep speed is produced both by spin and precession and assuming that the latest is slow compared to the spin speed (at least one order of magnitude slower), it is reasonable to expect that the component of the precession motion parallel to the spin speed component will be the more significant one in changing the accesses duration. Then, T_{mean} is corrected by a factor that depends on the spin and precession speeds, ω and Ω respectively

$$T^*_{mean} = T_{mean}f_{prec} = T_{mean}\frac{\omega\sin(\beta)}{\omega\sin(\beta) + \Omega\sin(\varphi)\gamma} \tag{21}$$

where γ is the angle between the projection of the precession velocity unitary vector over the spin velocity vector as shown in Fig. 10(a). This approximation is based on the fact that the precession motion modifies the speed of the instrument proportionally to its separation to the precession axis (φ). To obtain γ, the expressions of both unitary vectors are derived as a function of ϕ and τ angles, which are defined in Fig. 10(b)

$$v_{spin} = \left\{\begin{array}{c} \sin(\alpha)\sin(\phi) \\ \cos(\phi) \\ -\cos(\alpha)\sin(\phi) \end{array}\right\} \tag{22}$$

$$v_{prec} = \left\{\begin{array}{c} \cos(\tau) \\ 0 \\ -\sin(\tau) \end{array}\right\} \tag{23}$$

The relation between both angles is

$$\tau = \arctan\left(\frac{\sin(\varphi^*_{t_{max}})\sin(\phi)}{\cos(\alpha)\sin(\varphi^*_{t_{max}})\cos(\phi) + \sin(\alpha)\cos(\varphi^*_{t_{max}})}\right) \tag{24}$$

and γ is obtained projecting both vectors

$$\gamma = \cos(\phi)\cos(\tau) + \cos(\alpha)\sin(\phi)\sin(\tau) \tag{25}$$

where ϕ can be expressed as a function of φ, α and $\varphi^*_{t_{max}}$, which is the value for the maximum access time achievable (Bermejo-Ballesteros *et al.* 2022).

$$\phi = \arccos\left(\frac{\cos(\alpha)\cos(\varphi^*_{t_{max}}) - \cos(\varphi)}{\sin(\alpha)\sin(\varphi^*_{t_{max}})}\right) \tag{26}$$
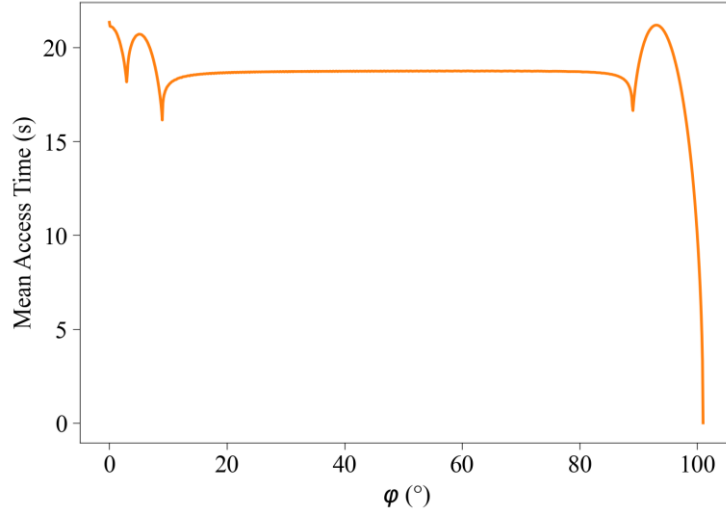
Fig. 9 Example of T_{mean} profile for negligible precession

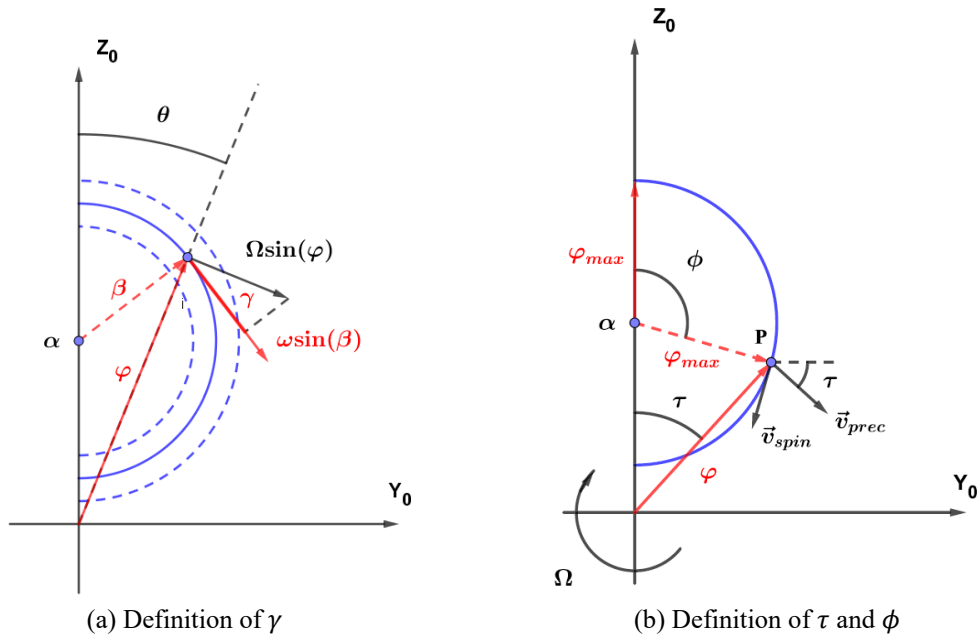(a) Definition of γ (b) Definition of τ and ϕ

Fig. 10 Geometrical scheme of the instrument trace for a half of T_{spin} when precession is negligible

$$\varphi^*_{t_{max}} = \arctan\left(\frac{\sqrt{\cos^2(\delta) - \cos^2(\beta)}}{\cos(\beta)}\right) \tag{27}$$

In Fig. 11 is shown the effect of the precession in the T_{mean} profile from Fig 9. The effect of the precession is more noticeable as φ grows, decreasing the value of T_{mean}.

In Fig. 12, the evolution of the value of the correction factor f_{prec} regarding φ, for different
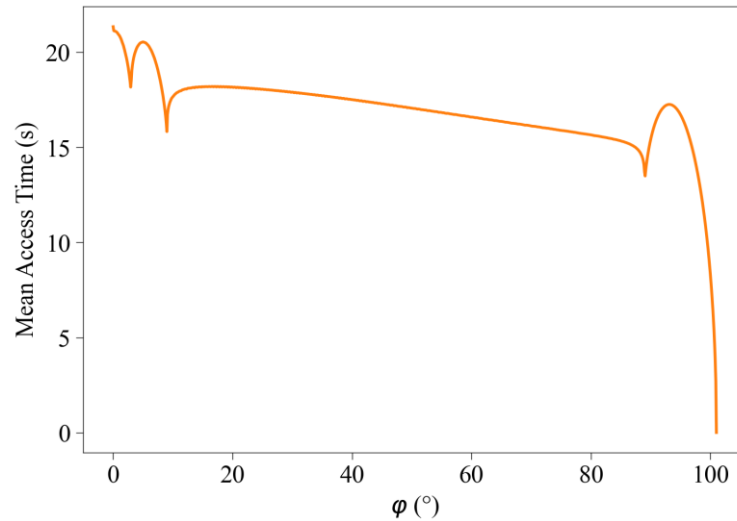
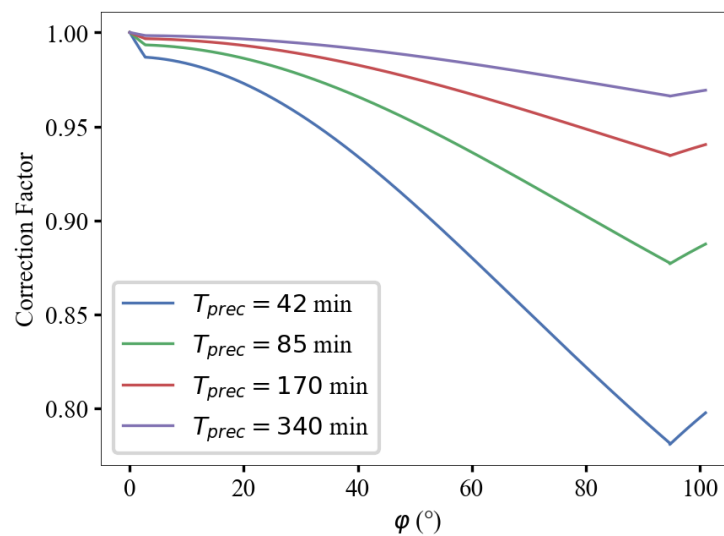Fig. 11 Example of T_{mean} profile after applying correction factor

Fig. 12 Value of the f_{prec} correction factor along the φ domain for different precession speeds

values of T_{prec}, is shown. Its value decreases until $\varphi = \alpha + \beta = 95°$, where it starts to grow, as the angular separation regarding the precession axis reduces again. In Fig. 13, a summary of the steps of this new approach is shown.

3. Results comparison

The new approach, due to the reduction of θ_e and θ_i to simple expressions, is considerable faster to compute that the original approach. In Table 1, the computation time used in both approaches is
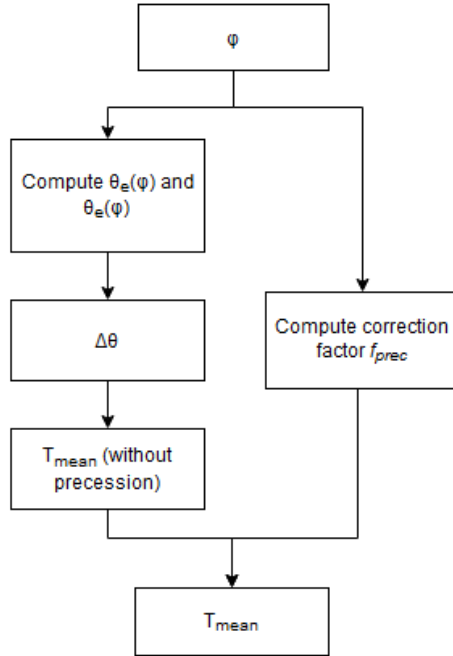
Fig. 13 Scheme of the steps followed to compute T_{mean} with the new approach

compared for different levels of φ discretization. The computer employed has an Intel® Core™ i7-10700K CPU of 3.80 GHz processor. In all simulated cases, the performance of the new method is over 100 times faster. Nevertheless, it must be noted that both methods are significantly faster than the numerical approach. For similar resolution in φ coordinate ($N_r = 1000$), 1 day of simulated time, and a time step of 1 s, the numerical approach consumes 1 h. As the computation times scales proportionally to the time step used, a time step of 0.1 s would require roughly 10 h of computation time. Unlike in the numerical approach, the computation time of analytical approaches does not depend on the simulated time.

For validation, both methods were compared to the numerical results for different values of T_{prec}. The scan strategy parameters used were $\alpha = 46°$, $\beta = 49°$ and $T_{spin} = 9$ min, similar to those used in CMB missions (Wallis *et al.* 2017). In Fig. 14 are shown the results of the three methods, which fit properly. In Fig. 15 the error of the analytical methods regarding the numerical is shown. For slow precession motion (T_{prec} large), both methods present similar error, with a RMSE (root-mean-square error) below the time step used in the numerical method (0.1 s). However, as the precession motion speed grows (T_{prec} decreases), the error of the new method becomes larger than with the original method. Note, however, that the error has roughly the same order of magnitude that the time step used in the numerical approach (0.1 s). This behaviour was expected as, contrary to the original method, which is derived from the analytical expression of the trace, the effect of the precession has been considered with an approximation of such effect. The four peaks of error present in both pictures from Fig. 15 are due to steep changes in the value of T_{mean}, which increases the error of the bilinear interpolation method used to process the numerical results and it depends on the level of spatial discretization used.
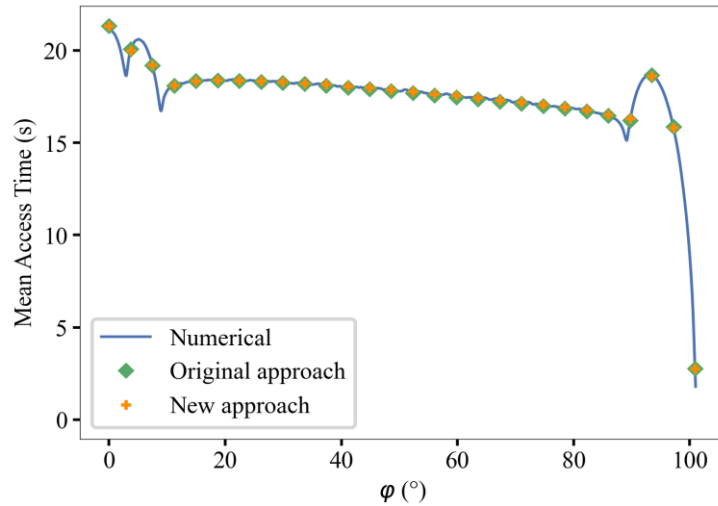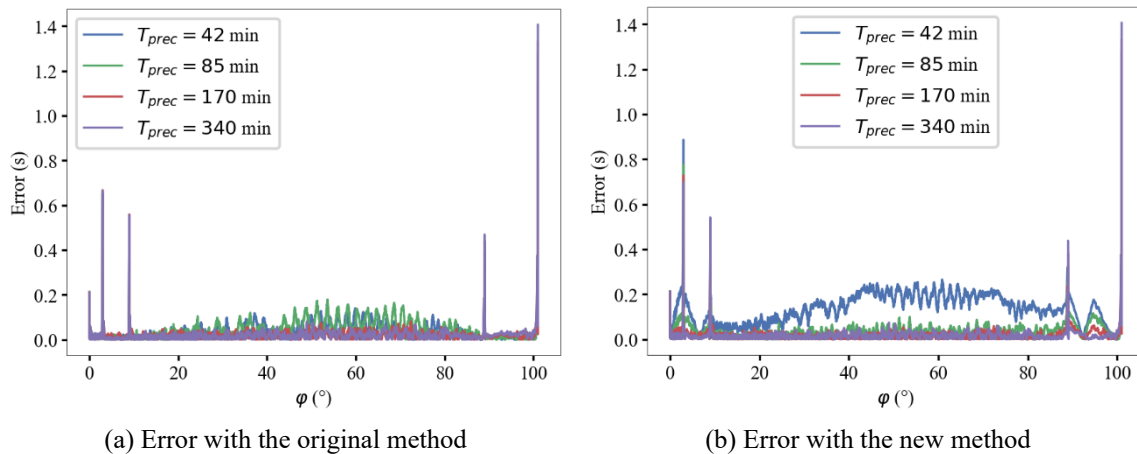
Fig. 14 Comparison between numerical results and both analytical approaches $T_{prec} = 85$ min.

(a) Error with the original method

(b) Error with the new method

Fig. 15 Comparison of the error between the numerical and analytical solutions for the original (a) and new method (b) for different values of T_{prec}.

Table 1 Comparison between both methods' execution times. Nr indicates the number of points in which the domain of φ is divided

Nr	Original method [ms]	New method [ms]	Ratio
10	70.49 ± 0.76	0.526 ± 0.008	133
100	674.6 ± 3.9	5.01 ± 0.02	134
1000	6642.3 ± 23.9 ms	49.62 ± 0.81 s	133

4. Conclusions

The new method has proven to be as accurate as the original for slow precession speeds. For large precession speed, the error will be higher. Nevertheless, whether the speed of the precession

motion can be considered slow or fast, and therefore, whether to expect higher error with the new method, will depend on its comparison with the spin motion speed. For precession speeds at least one order of magnitude slower than spin speeds, the error of both methods will be similar.

The new method proposed has been validated as an alternative to account for the precession motion in the computation of the mean observation time. This approach reduces the operations involved in the calculation and their complexity, avoiding the use of equation solvers, and thus decreasing the amount of time required in calculation and in the implementation process.

In terms of accuracy and computation time, both methods are adequate for a preliminary study phase, where the amount of time available for observation is a main driver for the mission design and it may require considering long periods of observation. In further design stages, numerical calculations are preferred as they enable the computation of other effects related to the signal itself and the instrument used to measure it.

Acknowledgments

References

Bennett, C.L., Bay, M., Halpern, M., Hinshaw, G., Jackson, C., Jarosik, N., ... & Wright, E.L. (2003), "The microwave anisotropy probe mission", *Astrophys. J.*, **583**, 1-23. https://doi.org/10.1086/345346.

Bermejo Ballesteros, J., García González, S., Cubas Cano, J., Casas Reinares, F. and Martínez González, E. (2019), "Development of a calibration satellite for a CMB telescope flying in formation about L2 libration point", *Proceedings of the 8th European Conference for Aeronautics and Aerospace Sciences*, Madrid, Spain. https://doi.org/10.13009/EUCASS2019-697.

Bermejo-Ballesteros, J., Cubas, J., Casas, F. and Martínez-González, E. (2022), "Visibility study in a chief-deputy formation for CMB polarization missions", *J. Astronaut. Sci.*, **69**, 651-691. https://doi.org/10.1007/s40295-022-00325-z.

Bock, J., Cooray, A., Hanany, S., Keating, B., Lee, A., Matsumura, T., ... & Tran, H. (2008), "The Experimental Probe of Inflationary Cosmology (EPIC): A mission concept study for NASA's Einstein inflation probe", arXiv preprint arXiv:0805.4207. https://doi.org/10.48550/arXiv.0805.4207.

Casas, F.J., Martínez-González, E., Bermejo-Ballesteros, J., García, S., Cubas, J., Vielva, P., ... & Sanz, A. (2021), "L2-CalSat: A calibration satellite for ultra-sensitive CMB polarization space missions", *Sensor.*, **21**(10), 33-61. https://doi.org/10.3390/s21103361.

Delabrouille, J., De Bernardis, P., Bouchet, F.R., Achúcarro, A., Ade, P.A.R., Allison, R., ... & Perdereau, O. (2018), "Exploring cosmic origins with CORE: Survey requirements and mission design", *J. Cosmol. Astropartic. Phys.*, **2018**, 14. https://doi.org/10.1088/1475-7516/2018/04/014.

Dupac, X. and Tauber, J. (2005), "Scanning strategy for mapping the Cosmic Microwave Background anisotropies with Planck", *Astron. Astrophys.*, **430**(1), 363-371. https://doi.org/10.1051/0004-6361:20041526.

Hazumi, M., Ade, P.A., Adler, A., Allys, E., Arnold, K., Auguste, D., ... & Nishibori, T. (2020), "LiteBIRD satellite: JAXA's new strategic L-class mission for all-sky surveys of cosmic microwave background polarization", *Space Telescopes and Instrumentation 2020: Optical, Infrared, and Millimeter Wave*, **11443**, 431-450. https://doi.org/10.1117/12.2563050.

Kelsall, T., Weiland, J.L., Franz, B.A., Reach, W.T., Arendt, R.G., Dwek, E., ... & Wright, E.L. (1998),

"The COBE diffuse infrared background experiment search for the cosmic infrared background. II. Model of the interplanetary dust cloud", *Astrophys. J.,* **508**, 44, https://doi.org/10.1086/306380

Wallis, C.G., Brown, M.L., Battye, R.A. and Delabrouille, J. (2017), "Optimal scan strategies for future CMB satellite experiments", *Month. Notic. Roy. Astron. Soc.*, **466**(1), 425-442. https://doi.org/10.1093/mnras/stw2577.